Optical Path Length Equalization

A. K. Garrison
GTRI, Georgia Institute of Technology, Atlanta, GA 30332

G.1. INTRODUCTION

The Optical Path Length Equalizer (OPLE) subsystem provides the variable delays necessary to keep the telescopes phased as they track an object under observation. This subsystem is a critical part of the CHARA Array. The basic CHARA design goal of simultaneously combining light from each telescope to form fringes requires that there be seven delay lines, one for each telescope. The length of a given delay line is determined by the longest baseline possible using its associated telescope. The number of delay paths and their lengths make the OPLE unique among the optical interferometers now in operation or under construction.

The following sections present the design requirements for the OPLE, a discussion of the functions of the OPLE, detailed descriptions of the subsystem assemblies and the results of several trade studies done to assess the risks associated with certain design options.

G.2. TEST BED EQUIPMENT

The design of the assemblies that move the mirror is based on measurements made on a laboratory prototype that was built for a test bed in the Phase A design study. The following is a description and presentation of the results of the experiments.

We chose a Thomson Roundway bearing early on in the design study for the retroreflector cart bearings. The design of the Roundway bearings provides semikinematic contact between the OPLE rails and car. Two vee-type bearings ride on one rail while a third single bearing rides on the other. The resulting five-point contact eliminates all but one degree of freedom: motion up and down the track. The cart cannot rock on its bearings with this design. The vee-type bearings prevent side to side shift of the cart, eliminating the need for a separate set of bearings and rails to constrain the cart laterally. Misalignments between the rails are easily accommodated by the self aligning design of the bearings.

As the bearings use only rolling contact, the coefficient of friction of the Roundway bearings is exceptionally low, 0.004 for single bearings and 0.007 for vee-type bearings. The dynamic coefficient is very nearly equal to the static coefficient which reduces the "stick-slip" effect present in many other bearing designs. The roller diameters can be matched at the factory to within 20 μm in producing an exceptionally smooth riding bearing. The simplicity of this design encouraged us to build a prototype OPLE during the design study.

The OPLE demonstrator was built to prove that the design achieves the required smoothness of operation and precision of positioning. The demonstrator was built on a 4×10 ft Newport optical table. The track consisted of two hardened and ground 2 in diameter steel Thomson Round Ways and the Roundway bearings described above. Each rail had a 4 ft and a 6 ft section so that the effects of track joints could be assessed.

In order to isolate the mirror carriage from disturbances introduced by the power train, a "tractor-trailer" concept was employed. A third T-shaped rail was mounted between the

two precision rails; the tractor traveled by friction drive on this low precision rail, towing the mirror carriage riding on the Roundway bearings. The "towbar" connection between the tractor and the carriage was made of self-aligning precision rod end bearings, ensuring that the only effect the tractor can have on the trailer is a straight pull down the track. It is conceded that speed variations can be transmitted to the mirror carriage, but these were minimized by use of a microstepped stepper motor, a 60:1 speed reducer, and by ensuring that the drive wheels were as circular as possible.

Initial tests with a flat mirror mounted on the mirror carriage and a Nikon autocollimator showed the mirror carriage tilted 2 to 3 arcminutes as it rolled down its 10 ft track. At that point the rails had been aligned with the surface of the optical table with a dial indicator reading to 1/10000 of an inch. Further adjustments of the rail mounts according to autocollimator readings reduced the tilt to about 30 arcseconds over most of the track length. Further attempts at reducing the tilt error actually increased it. The alignment difficulty was traced to crosstalk between the horizontal and vertical adjustments in the Round Way mounts, and also to the rails floating free in the mounts. Thomson Industries has a mount configuration which ties the rails to the mounts. This may make alignment somewhat easier.

A series of tests were made to quantify the vibrational spectrum of the mirror cart as it moved up and down the rails. A magnetic accelerometer with a sensitivity of 90mV/g was attached to a ferrous plate and placed next to the coupling on the mirror cart. The accelerometer was arranged so that it was sensitive only to motion parallel to the rails. The output of the accelerometer was amplified by a Tektronix Differential Amplifier, model AM 502, which had a bandwidth from DC to 1 MHz and then analyzed by a Hewlett Packard Spectrum Analyzer, model 3582A, with a response from 0.02 Hz to 25.5 kHz.

The cart was driven along the track at a selected speed, and the vibrational spectrum was averaged by the spectrum analyzer for the entire trip. The averaging was started after the cart had damped out any start-up transients. At the end of the run the output of the analyzer memory was recorded with an $x - y$ plotter, and the procedure was repeated for the same speed in the opposite direction. Motor speeds from 1 to 5 rps (corresponding to cart speeds of about 5 to 26 mm/sec) in steps of 1 rps were used.

It was found that the mirror cart resonated with the stepper motor for speeds above 2 rps. Typical spectra are shown in Figure G.1. The accelerometer was not well calibrated over the frequency range so the peak voltage of the resonances could not be translated into a corresponding amplitude of the cart vibration. However, it is significant that the resonance maxima were consistently smaller for motion in the negative direction. For a speed of 4 rps in the negative direction, the resonances were not large enough to measure. As seen in Figure G.1, the resonances were not observed in either direction for speeds of 1 and 2 rps. Attempts were made to examine the details of vibrations around 0.18 Hz by narrowing the frequency range.

These results suggested several modifications of the OPLE cart design. Isolating the drive trolley from the mirror cart at the coupler and mounting the motor in the center of the trolley should help reduce the vibrations and their transmission to the mirror cart. The directional effects are attributed to the worm gear in the drive trolley so this should be replaced by a steel belt or other type drive that does not give a directional effect.

Another series of measurements was made to determine with high accuracy the position of the cart as a function of time as it moved on the rails in order to assess the requirements for a correction system that would maintain the mirror cart position to within 2 μm of that

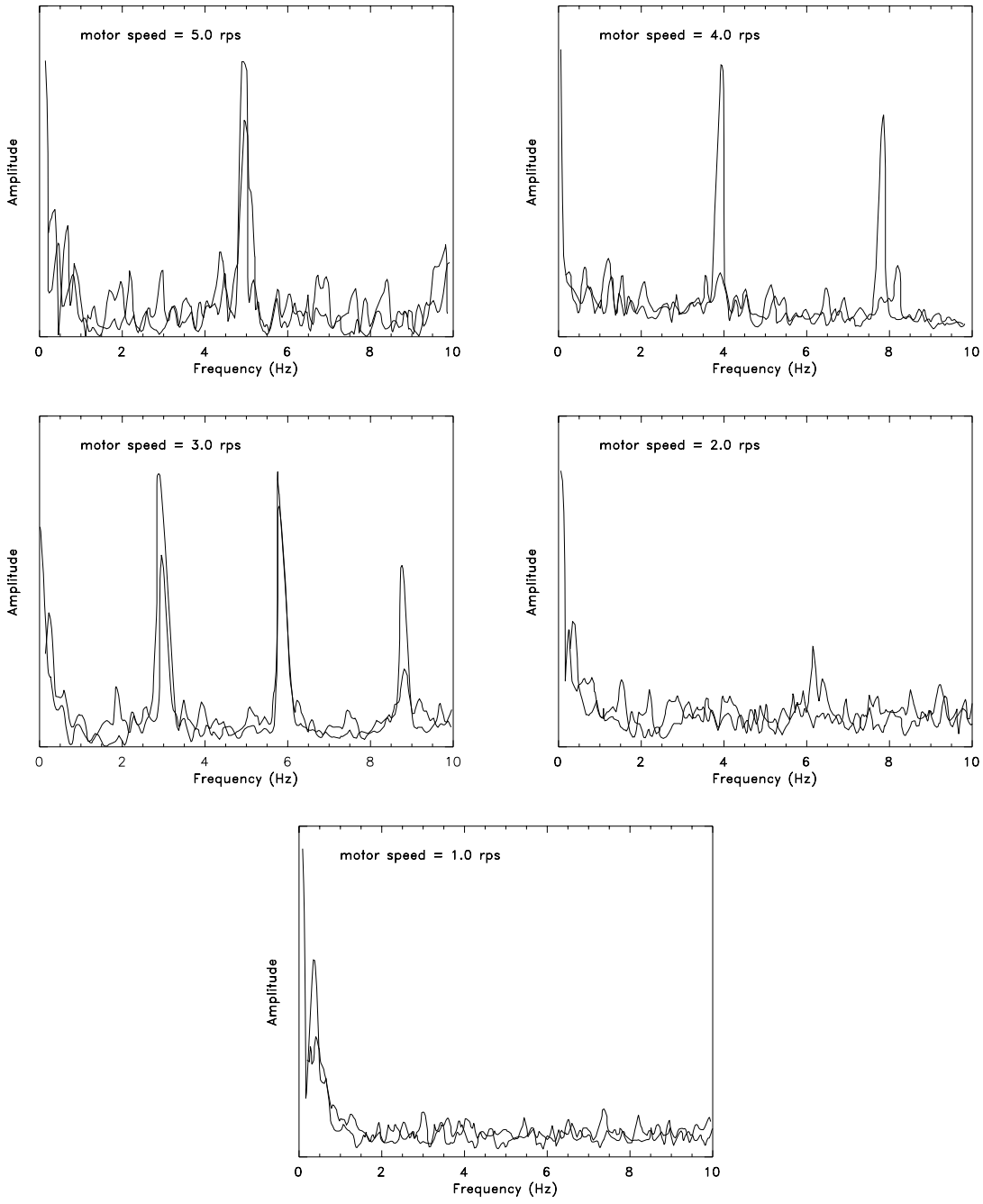

FIGURE G.1. OPLE prototype cart vibration spectra.

required for the desired fringe visibility.

A Teletrac TIPS IV-MT laser interferometer was used to measure the position of the cart by placing one of the retroreflectors on the mirror cart. The interferometer consisted of a single mode HeNe laser that had a frequency control with a short term stability of 1 Mhz/s and a long term stability of 10 Mhz/24 hrs., a beam splitter and fixed mirror unit and the counter-display unit. The resolution of the instrument was 79 nm and the accuracy of the 10 digit display was 1 PPM or 10 nm. The interferometer compared rotations of a circularly polarized beam between the moving and fixed mirror to obtain the accurate and consistent distant measurements.

The position measurements were read into a PC file using the RS 232 serial port on the counter-display unit. The rate of reading was controlled by a TTL pulse generator, but the internal timing of the counter-display prevented a rate faster than one every 100 millisecond. Thus a record of position versus time was made for each run.

The cart was driven at a selection of uniform speeds from 5.22 μm/s to 26100 μm/s and the position versus time was recorded as described above after the start-up transients had damped out. A least-squares fit to the straight line of the uniform speed was made and the residuals calculated for each speed. The sum of the residuals was checked in each case to be zero. Graphs of the position errors from those for a constant velocity are shown in Figures G.2 and G.3. Points that obviously were off from the trends were thought to be erroneously recorded positions because the readout from the counter was occasionally requested by the computer before the proper value was available. These points were excluded from the data analyses.

A frequency analysis of the position deviations was also done via the Fast Fourier Transform. Note that the Nyquist frequency due to the 0.1 sec sampling time is 5 Hz. Figure G.4 shows the frequency response from several representative cart speeds. Clearly, the cart motor was a significant source of vibration (as found from the accelerometer results). In addition, there was a low-frequency rumble at 0.1–0.2 Hz also observed with the accelerometer.

The total power spectrum (square of amplitude) above 0.2 Hz is plotted as a function of motor (and cart) speed on Figure G.5. Note that the relation is nearly linear except at very low speeds. The data are scaled to the rms amplitude variation (scaling checked by inputting sine waves into the program). Given the maximum cart rate of 0.4 cm/s, the worst case rms vibration is about 3 μm. For comparison, the atmosphere, moving at 5 m/s would create a comparable 5.7 μm rms position error at a 1 Hz frequency ($r_\circ$= 0.1 m, λ = 550 nm).

In summary, the cart observations in this prototype experiment are encouraging, especially because a number of improvements can be easily made to reduce vibration.

The promising results of the tests on the prototype OPLE cart and the performance of a similar optical path length compensator used in the Sydney University Stellar Interferometer (SUSI) form the basis for the design of the OPLE. Figures G.6 and G.7 show the OPLE subsystem hardware tree to the assembly level to illustrate the structure of the design. The following sections provide the details of each of the assemblies.

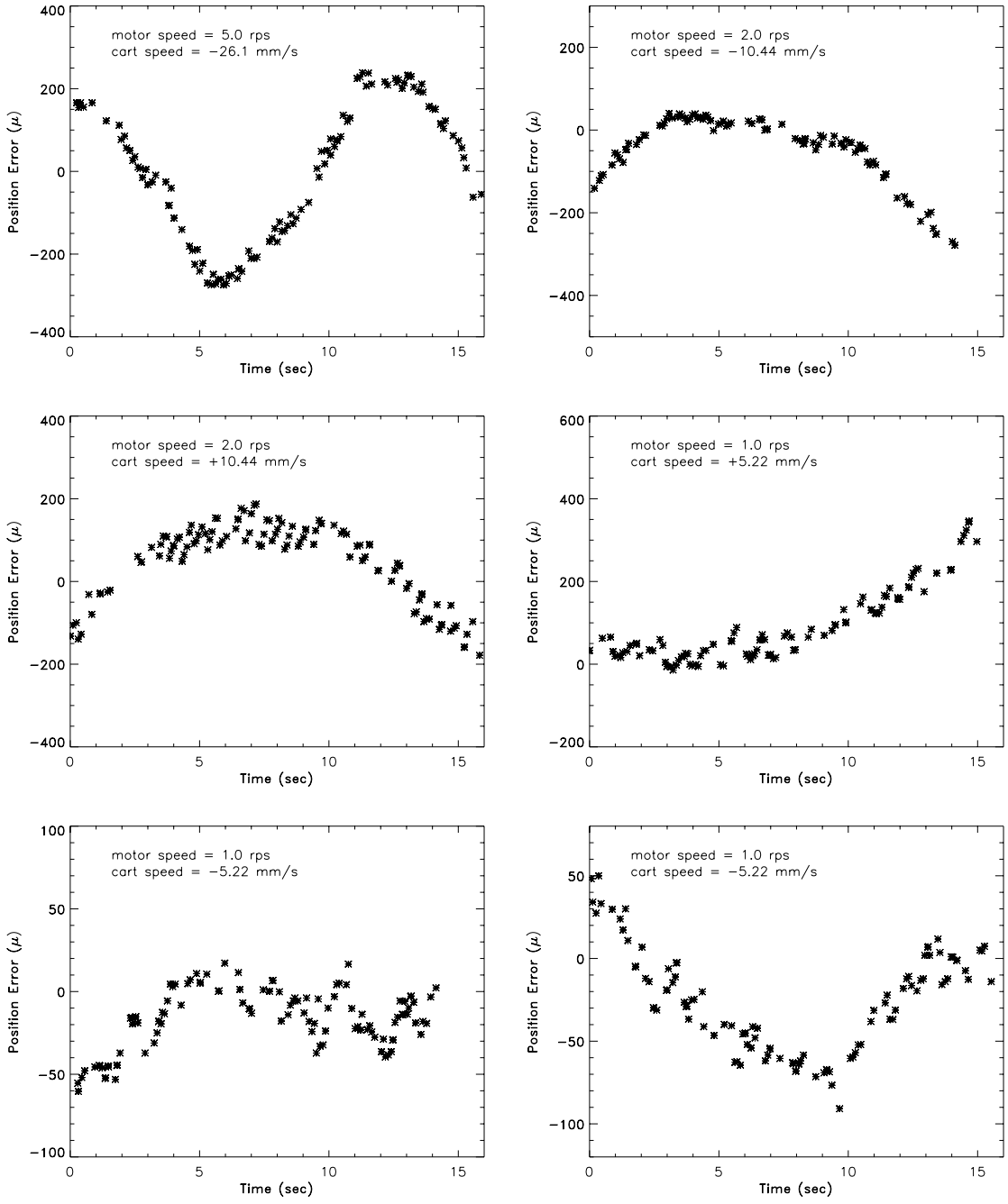

FIGURE G.2. OPLE prototype cart position errors.

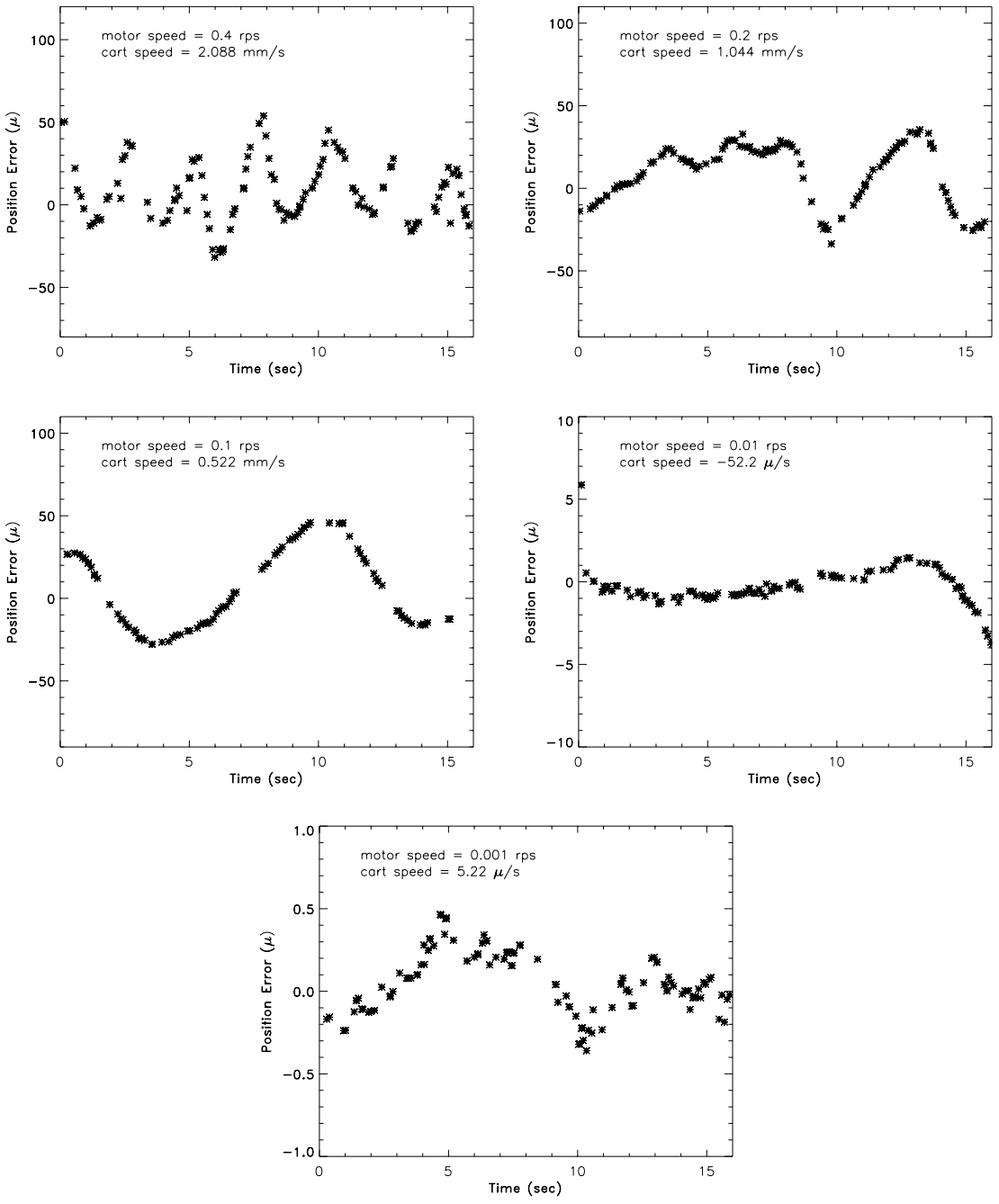

FIGURE G.3. OPLE prototype cart position errors (continued).

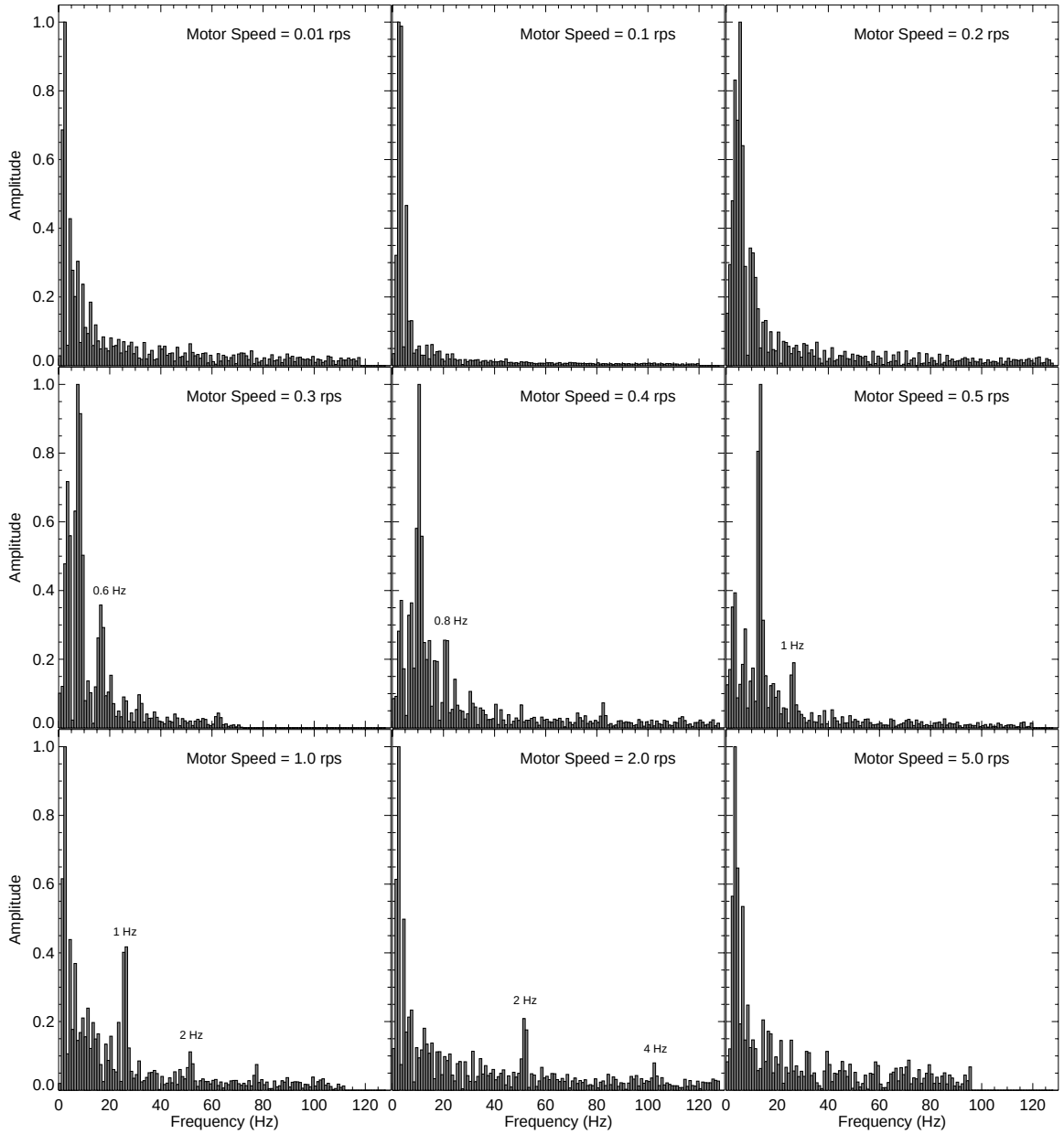

FIGURE G.4. Frequency response of the OPLE prototype cart from position measurements for various motor speeds.

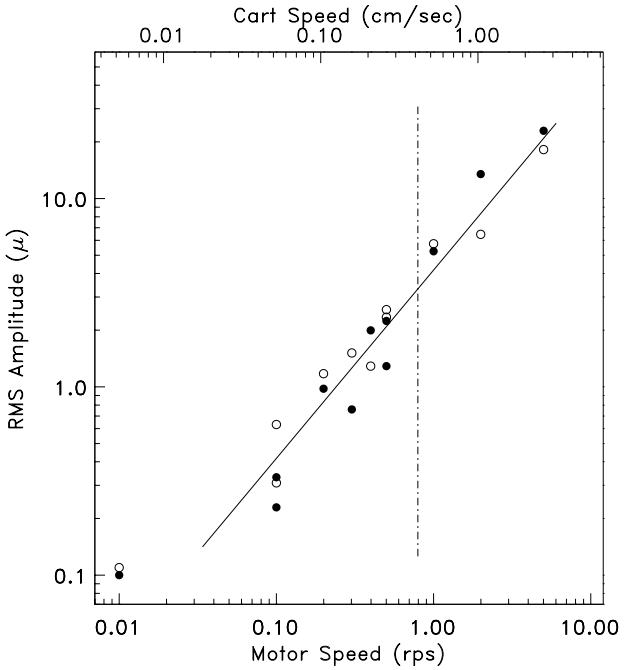

FIGURE G.5. OPLE prototype cart power spectrum, as a function of motor speed. Positive and negative cart speeds are shown as filled and open circles, respectively. The projected maximum cart speed is indicated by the vertical dot-dashed line.

G.3. OPLE SUBSYSTEM

G.3.1. System Requirements

The subsystem requirements are:

1. Equalize the optical path length from each telescope while tracking objects between 1.5 and 50 degrees zenith angle.
2. Meet requirement 1 over the visible (0.4–0.9 micron) and IR (0.9–2.5 micron) wavelength regions.
3. Meet requirements 1 and 2 so that the uncorrected path differences shall not exceed a value determined by the system requirement that the visibility accuracy be $\Delta|V^2| \leq 0.05$ on a scale of 0–1.
4. Meet requirements 1, 2, and 3 under temperature variations of $\pm 1^\circ$ C, pressure variations of ± 0.1 mm Hg and relative humidity changes of $\pm 1\%$.
5. Slew to new starting positions within 5 minutes.
6. Maintain a subsystem reliability so that there are at least 200 operational hours between failures.
7. Meet any requirements for the safe operation of the subsystem.

G.3.2. OPLE Subsystem Overview

The basic features of the OPLE are a cat's eye mirror assembly that moves under control of a fringe tracking system on precision rails and a fixed mirror assembly at one end of the

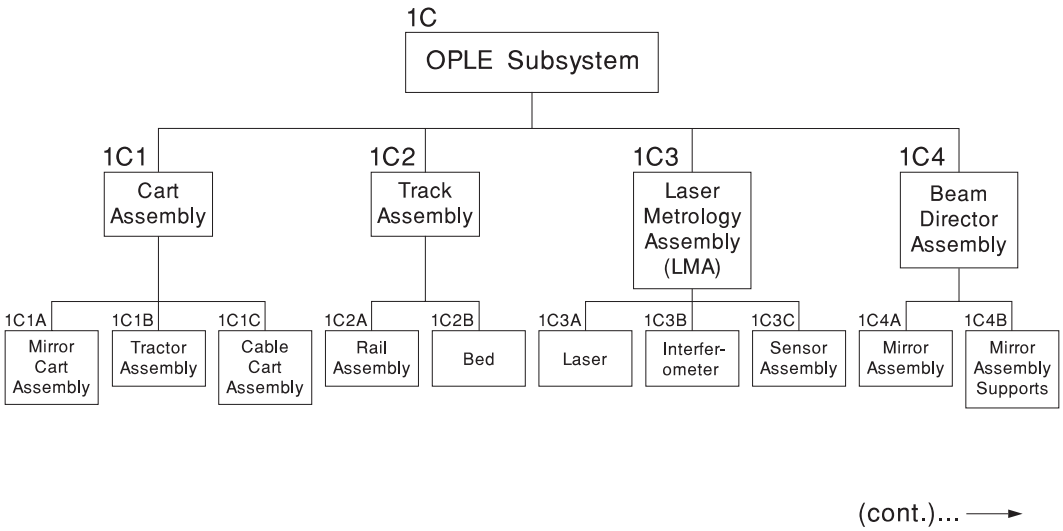

FIGURE G.6. The OPLE subsystem hardware tree (continued in the following figure).

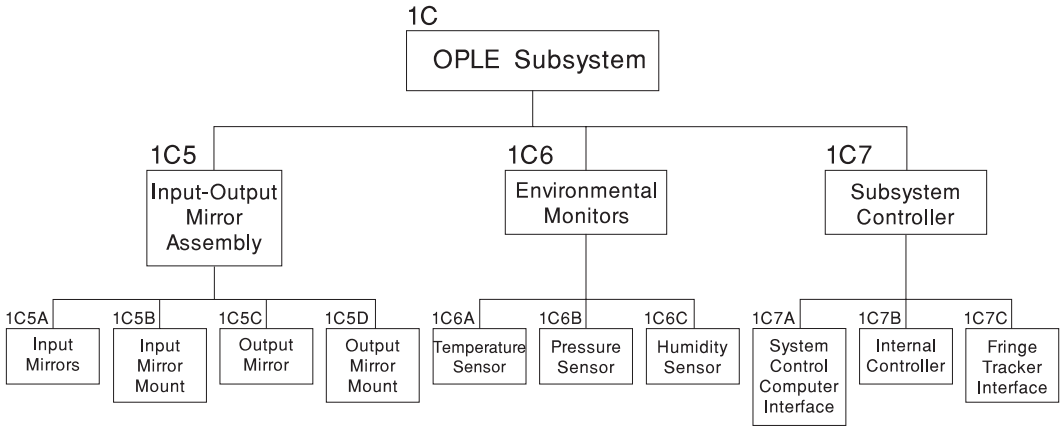

FIGURE G.7. The OPLE subsystem hardware tree (continued).

rails that relays the light beams four times along the distance between the fixed mirrors and the moving cat's eye assembly. The position of the mirror assembly with respect to a fixed reference is continuously measured with a laser interferometric metrology assembly (LMA). There are seven moving mirror assemblies each with it own track, fixed mirrors and LMA. The seven tracks will be placed side by side with each track on a bed that is isolated from seismic and other vibrations. The OPLE will operate in air in an enclosure within a building. The heating and air conditioning ducts will be in the volume between the OPLE enclosure and the walls of the building so that the air in the OPLE will have little disturbance.

Figure G.8 shows the placement of the OPLE subsystem with respect to the other subsystems of the array. The beams from each of the ten possible telescope positions will be directed to one of the seven OPLE tracks by a beam director assembly which will be described in more detail later.

FIGURE G.8. The telescope/OPLE layout.

The lengths of the OPLE fixed-mirror distances are determined by the projection of the unit position vector to the object that is observed on the position vector of the telescope that is being phased plus the distance from the OPLE to the telescope. The maximum and minimum lengths are determined by the maximum of the zenith angles specified in requirement 1. These calculations lead to the lengths shown in Figure G.9. The vertical lines represent the OPLE track length that will provide phasing of the telescopes designated in the boxes beside the vertical lines. The first letter specifies the telescope configuration and the second letter specifies the telescope position as shown in Figure G.8. This arrangement will allow phasing of all seven telescopes in configuration A or B. All the tracks will be extended to start at zero to provide for the cases where a small number of telescopes are phased together.

G.4. ASSEMBLY DESCRIPTIONS

G.4.1. Cart Assembly

The cart assembly consists of the mirror cart which carries the cat's eye mirror assembly, the tractor cart which moves the mirror cart and the cable cart which is slaved to move with the tractor cart and pulls the power and control cables to the cart assembly. The functions of the cart assembly are to provide a smoothly moving mirror to correct for the time varying optical path difference from each telescope and to provide means to correct

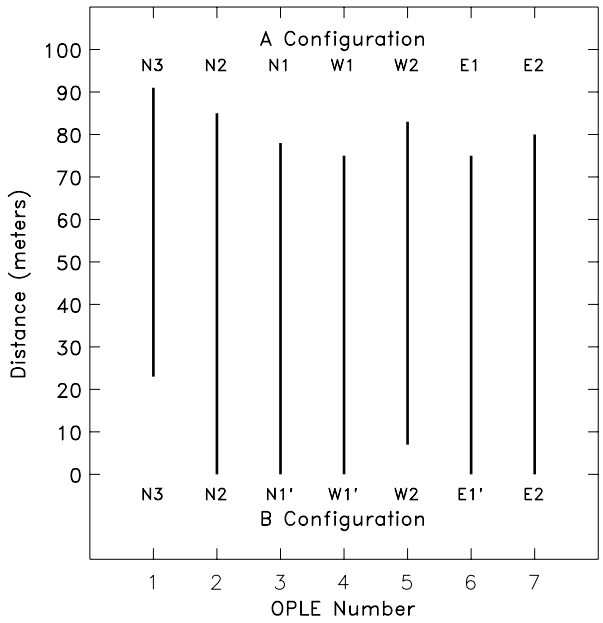

FIGURE G.9. OPLE track lengths and relative positions.

for the time varying piston distortion of the wavefronts introduced by the atmosphere and the telescope tracking. Figure G.10 shows a drawing of the cart assembly design concept. There are seven of these cart assemblies, one for each operating telescope. All the carts will have a honeycomb aluminum panel base to reduce vibration and weight and the Thomson linear bearings to match the precision rails that were used in the prototype. The following paragraphs discuss the functions and design details of each part of the cart assembly.

G.4.2. Retroreflector

The retroreflector on the mirror cart is a cat's eye consisting of a paraboloid f/3 mirror with 34 cm diameter and 31 cm clear aperture to accommodate four reflections of the 12.5 cm beams from the telescopes. The secondary is a 1 cm diameter plane mirror. Another retroreflector design consisting of a moving dihedral with a horizontal axis of symmetry and a dihedral with a vertical axis of symmetry fixed at the other end of the OPLE track was compared with the cat's eye. The comparison was a study of the effect of infinitesimal rotations of the moving mirror about an axis parallel to the OPLE rails and the two axes perpendicular to the rails on the direction of the retroreflected beam using analytical ray tracing. In the analysis of the cat's eye the beam reflected off the paraboloid, then the plane mirror, and then the paraboloid again. For the dihedrals analysis, we had the incoming beam reflect from each of the dihedral surfaces so that the incident and reflected beams are in a vertical plane, then reflect off the stationary dihedral so that the incident and reflected beams are in a horizontal plane, and finally reflect off the moving dihedral again to give a retroreflected beam. For incoming beams exactly parallel to the rails, both systems do not deviate the retroreflected beam with rotation of the moving mirror about an axis parallel to the rails. (This rotation arises because the two rails are not at the same height.) The cat's

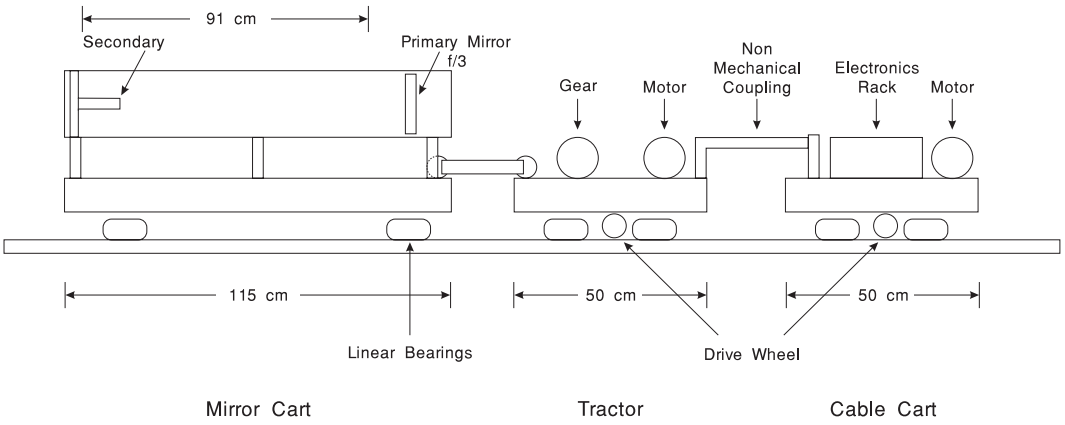

FIGURE G.10. The OPLE cart assembly design concept.

eye does not deviate a return beam due to rotation about an axis parallel to the rails, even if the beam is not parallel to the rails, because of its symmetry about that axis, whereas the dihedral configuration does mix the rotation with the off-axis components of the incoming beam to give a deviated outgoing beam. For this reason, and because the cat's eye has a secondary that can be used for piston correction, the cat's eye was chosen over the dihedral configuration.

The amplitude and frequency of the atmospheric piston distortion of the wavefronts depends on the "seeing" conditions and the wavelength. However, for the purposes of specifying the range of the rms of the variance of the amplitude of the piston versus frequency, it is sufficient to use the shortest wavelength to be used by the array, 500 nm, and typical seeing of $r_\circ = 10$ cm. These conditions give a range for the variance of the amplitude of 10 μm for frequencies greater than 0.01 Hz to 0.01 μm ($\lambda/50$) for frequencies greater than about 5 Hz. The amplitudes will be smaller for longer wavelengths. Thus any system that corrects for the atmospheric piston must have at least this type of amplitude versus frequency spectrum.

The active elements to correct the piston errors consist of three different devices that cover the amplitude-frequency spectrum described above. The stepper motor on the tractor assembly will cover the amplitude range above 10 μm in the frequency range below 1 Hz. A piezoelectric ceramic stack transducer (PZT) that displaces the cat's eye flexure assembly mount will cover the amplitude range from 1 μm to 15 μm and the frequency range from 0.1 to 2 Hz. The final correction is achieved by a PZT transducer displacing the secondary plane mirror in the amplitude range from 0.01 to 1.5 μm in the frequency range from 1 to 10 Hz. (Physical movement of the stepper and flexure by $\pm x$ changes the optical path by $\pm 4x$, whereas the same change in the physical movement of the secondary changes the optical path by $\pm 2x$.) The requirement for the stepper motor are well within the specification of the tractor as will be discussed below. The requirements for the PZT transducers are within typical specifications for PZT which have maximum travel in the mm range, mechanical resolution in the 1 nm range and maximum speeds in the 1 mm/s range.

The movement of the secondary mirror will introduce a slight beam steering and defocus. The size of these effects were estimated using GENII-Plus ray tracing software. The effects are nearly linear for micron displacements of the mirror. For the maximum displacement of 1.5 μm, the wavefront will tilt $0\farcs6$ toward the paraboloid axis when the secondary moves away from the primary. The marginal rays increase their convergence by $0\farcs08$ for the same

movement of the secondary.

The mirror cart also contains a device to sense a reference position for the calibration of the optical path length difference before a measurement. The sensor is based on magnetic induction and consists of a magnet on the cart and a set of coils at the reference position on the rails. The sensor can relocate the cart to within a micron of the reference position.

G.4.3. Tractor Assembly

The tractor assembly uses a microstepper motor that has 25,000 steps per revolution, a gear reduction of 1/60 and a drive wheel four inches in diameter so that one microstep is 0.21 μm. The maximum speed of the stepper is 2,000 rpm which can give a slewing speed of 17 cm/s. It is estimated that a slew speed of 12 cm/s will allow a cart assembly to traverse half the longest track in less than five minutes. The drive wheel will work against one of the rails instead of a central flat rail as in the prototype. The coupler to the mirror cart will be redesigned from that used in the prototype to reduce the vibrations at the harmonics of the stepper motor rotational speed. The size of the microstep and the maximum speed of the motor indicate that the tractor will meet the requirement stated above for the piston correction.

G.4.4. Cable Cart Assembly

The cable cart is designed to pull the necessary power and signal cables from a stationary point at the middle of the track to the moving cart assembly without introducing significant error in the OPLE correction functions. The design is an adaptation of the one used in SUSI. The cart contains its own microstepper motor, gear reduction and drive wheel. However, the cart is slaved to the tractor cart by use of an active coupling between the two carts. The active coupling uses a light emitting diode (LED) on one side of a small aperture in the coupling bar that is attached to one cart. On the other side of the aperture is a photodiode that senses the amount of light through the aperture to get a control signal for the stepper motor. The cable cart also carries the electronics for all the systems on the entire cart assembly. The cable cart can be a significant source of thermal turbulence in the air path of the OPLE. It is placed as far away from the cat's eye as possible to minimize these effects, but other measures may be necessary if this turbulence is still a problem.

Figure G.11 shows a schematic of the cable feed assembly for the cable cart. The fixed pulleys are at the ends of the tracks, and the cables are fixed at the center of the track and on the cart. As the cable cart moves from one end to the other it also moves from one movable pulley to the other. The mass of the movable pulleys, rigging cord, cart and cable and friction in the pulleys must be small enough that the cable cart motor can pull it and keep slaved to the tractor. The torque from a medium size motor is in the 1 N-m range which corresponds to 20 N for a 2 in drive wheel radius. The maximum friction forces are estimated to be 10 N. If the maximum acceleration is that to get the cart assembly from rest to slew speed in 2 s, then the net accelerating force will accelerate 125 kg, or much more than the combined masses.

Figure G.12 shows the cart subassemblies hardware tree with each of the major parts listed. This provides a summary of the discussion of the cart assembly.

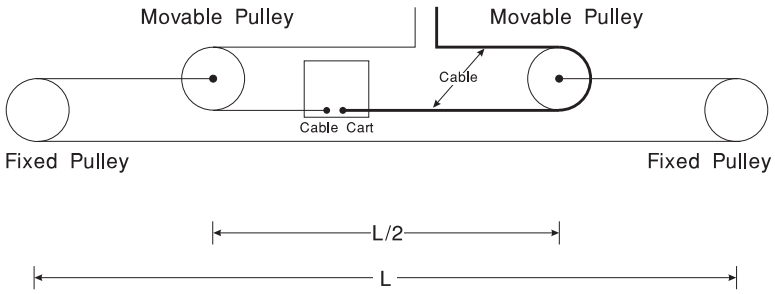

FIGURE G.11. The OPLE cable feed assembly, as adopted from SUSI.

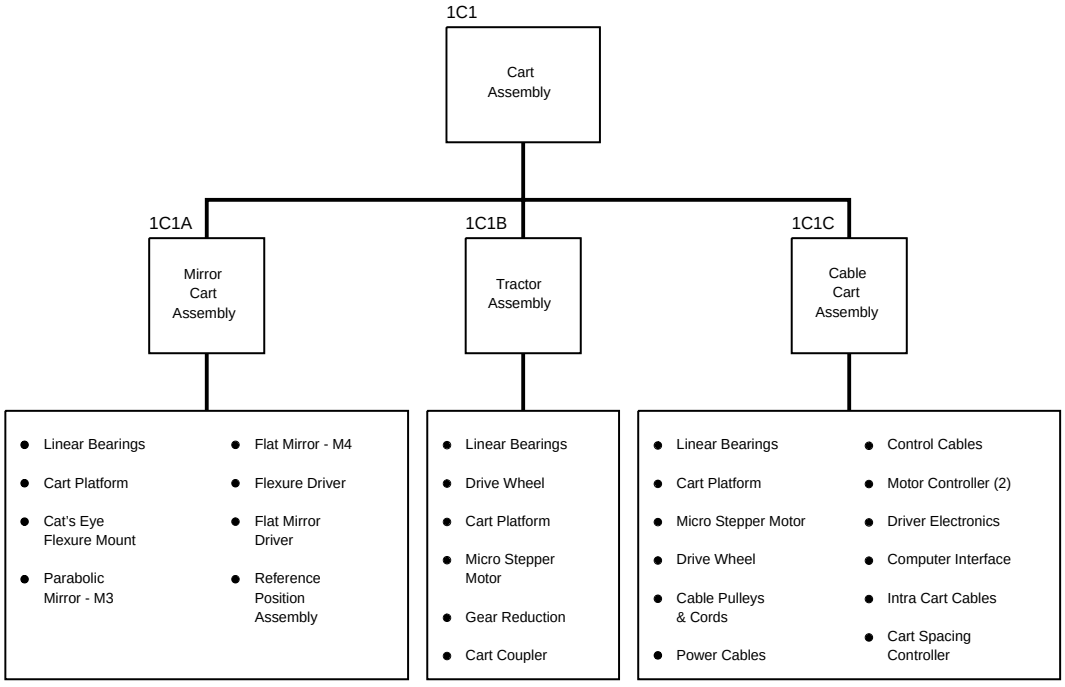

FIGURE G.12. The OPLE cart subassemblies hardware tree.

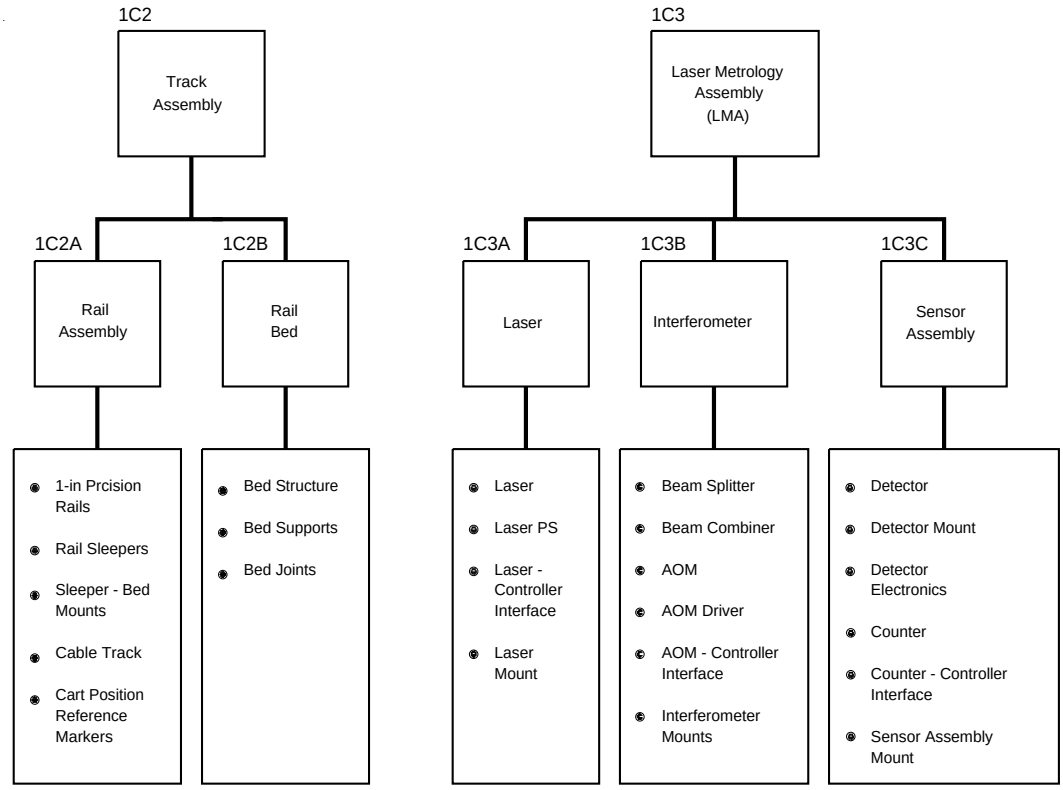

FIGURE G.13. The OPLE track and LMA subassemblies hardware trees.

G.4.5. Track Assembly

The track assembly consists of the rail assembly and the rail bed. Figure G.13 shows the subassembly hardware tree for the track assembly. The rail assembly has two 1-in diameter Thomson precision rails about 40 cm apart that run the length of each OPLE path. The rails will be obtained in 20 ft lengths with a tapered dowel-type joint. Thomson will make each joint and then regrind the surface at the joint to assure a smooth transition across the joints. Rails that were 2 in in diameter were used in the prototype test bed, but SUSI's experience with 1 in rails lead us to choose the smaller diameter. We will design and build our own rail sleepers to give independent adjustment in the separation and height of each rail. Likewise we will supply the sleeper to bed mounts. A cable track to protect the cart cables that move along the tracks will also be fastened to the track bed beside the rails. The coils for the magnet position reference sensor will also be fastened onto one of the rails to work with the corresponding part on the mirror cart.

Alignment of the rails will use a method similar to the method developed by the SUSI group. Initial alignment will use a taut wire along the complete length of the rail and jigs to compare the separation and height. A laser beam is used to trace along the track to get fine adjustment of separation and height. Finally, high resolution electronic leveling equipment will be used to make very fine vertical adjustments. This method gave SUSI a maximum height variation between any two sleepers of 245 μm and an average variation of about 100 μm as measured with a theodolite at intervals of every other sleeper.

Several designs for the rail beds are under consideration. It is fairly certain that the beds

FIGURE G.14. The OPLE track and track bed concept.

will be concrete, but whether the bed will be one continuous pour with expansion joints or whether there will be a series of discrete sections will be determined by a trade study comparing the cost and rigidity of the two concepts. It is assumed that the bed will go down to bed rock and not be tied to the floor of the building, but a final decision awaits geological assessments of the site and building design. Figure G.14 shows a drawing of two of the seven OPLE mirror carts, rails and rail beds with approximate sizes for some of the dimensions. The complete OPLE subsystem will be constructed by repeating the pattern shown in the figure for seven tracks side by side.

G.4.6. Laser Metrology Assembly

The laser metrology assembly (LMA) provides accurate position and velocity measurements of each of the carts as a function of time, interfaces with the system control computer to provide this information for the system operator and for archiving for use in data analysis. The LMA must make these measurements during slewing to start positions as well as during data runs. The hardware tree for the subassemblies of the LMA are shown in Figure G.13.

Table G.1 summarizes and quantifies the factors affecting the precision of metrology using laser interferometry. The first column of the table contains two values of laser frequency stability that are quoted by laser manufactures for times of 1 hour and 10 minutes. The next column gives the best available precision one would obtain in converting the vacuum wavelength to that in air. This limit is determined by the precision of the measured value of the index of refraction of air. The next three pairs of columns show the effects of

TABLE G.1. LMA Source of and Magnitude of Errors.

Laser Stability	$\frac{\Delta n}{n}$	$\frac{\Delta n(T)}{n}$	ΔT	$\frac{\Delta n(P)}{n}$	ΔP	$\frac{\Delta n(H)}{n}$	ΔH	Turbulence nm	Total Error x = 90m
	$\lambda_n \rightarrow \lambda_{\rm vac}$		°C		mm Hg		%	$\sqrt{\langle \Delta X_t \rangle^2}$	$\sqrt{\langle \Delta X_T \rangle^2}$
$1 \cdot 10^7$ (1 hour)	$5 \cdot 10^8$	$1 \cdot 10^6$	± 1	$3.5 \cdot 10^8$	± 1	$1 \cdot 10^8$	± 1	$30\sqrt{X(m)}$	$20\,\mu$m
$2 \cdot 10^8$ (10 min)	$5 \cdot 10^9$	$1 \cdot 10^8$	± 0.01	$2 \cdot 10^8$	± 0.02	$5 \cdot 10^7$	± 0.5	$30\sqrt{X(m)}$	$5\,\mu$m

temperature, atmospheric pressure, and relative humidity variations on the precision of the index of refraction of air and therefore on the precision of the measurements. The values in columns two, three, five, and seven are from Estler (1985). The two rows give typical changes in an hour and in 10 minutes. The ninth column gives an estimate of the rms error in the length measurement in nanometers due to enclosed air turbulence as a function of the path length. This expression comes from a private communication from G. Wyntjes of OPTRA, Inc and from data in the paper by Estler. The last column gives the rms error for a measurement of 90 m due to all the errors. The second row gives the maximum precision for converting to the laser wavelength in air as estimated by Estler. The variations in T, P, and H in the second row are the limits of accuracy for measurements of those quantities. Thus the most accurate measurement one can expect from the LMA for a path length of 90 m is the 5 μm listed in the last row, last column. The 20 μm value is taken as a typical error and implies that a band pass of about 15 nm is required in order to keep the coherence length of the telescope beams within this value (so that fringes can be found initially by using the LMA alone).

In addition to the frequency stability requirements of the laser stated above, the wavelength is equally important since it cannot interfere with the science beam. Most commercially available laser metrology interferometers use the 633 nm HeNe line which is in the middle of the visible observation band. We considered using a Rugate reflection filter to keep the 633 nm light from the fringe sensor, but no supplier would guarantee that the filter would not distort the wavefront for the non-filtered wavelengths. Of course, the metrology beam would not follow the same path as the science beam, but the metrology beam would be at least 10^6 times more intense than the science beam and we cannot assure ourselves that scattering would not contribute to mixing the two beams. The 633 nm wavelength was thus ruled out. There are interferometers that use laser diodes that have emission in the near infrared, but these are still in the development stage and were considered not reliable enough for this application. There is a commercial system that uses a 1.13 μm HeNe laser with the required frequency stability that would allow the science beam to cover the visible spectrum, and the IR from 0.7 to 1 μm and from about 1.2 to 2.5 μm. This keeps all of the visible and important parts of the IR system requirements available for science. This laser is the present choice for the LMA.

The interferometer beam will proceed from a beam splitter at the beginning of the OPLE track to the paraboloid of the cat's eye to the secondary, back to the paraboloid and then to the beam combiner next to the beam splitter. Figure G.15 shows the paths for the science and LMA light beams for one OPLE. In this arrangement the interferometer will

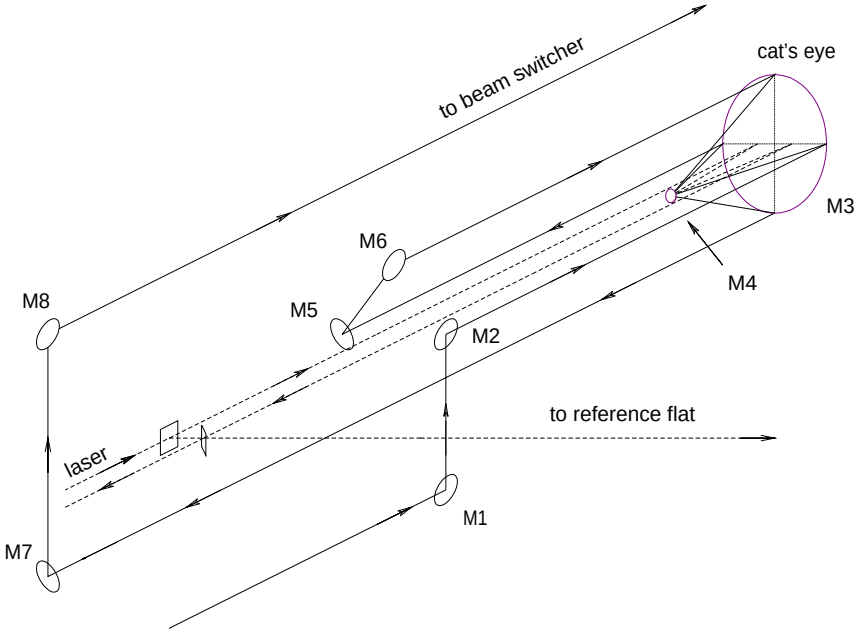

FIGURE G.15. Light path for the science (solid line) and LMA (dashed line) beams for one OPLE.

measure the physical position and velocity of the OPLE mirror cart on the rails and not the optical path length difference which is four times the measured values. The laser beam will have to have a small enough diameter and divergence so that it will follow this path and not be vignetted by the cat's eye secondary, but also not interfere with the science beams. This will require a beam expander to reduce the typical laser beam divergence from about 1.0 milliradian to 0.1 milliradian so the beam remains on the order of 1 cm in diameter at the largest OPLE cart positions.

The LMA sensor counting system must be fast enough to monitor cart slewing speeds of about 12 cm/s to meet the slewing requirements stated above. This can be accommodated by not requiring the accuracy for slewing that is required for tracking where the maximum speed is about 6 mm/s which can be measured at full accuracy. The other requirement of the sensor electronics is that the counter must be able to hold the number of counts for the long path lengths. This can be met by extending the counter memory or using the control computer to keep track of the overflow counts.

G.4.7. Beam Director Assembly

The beam director assembly uses mirrors to direct the light from the beam transfer subsystem into the OPLE. It also uses a set of movable mirrors to match the beam transfer tubes from the alternate positions for the movable telescopes to the proper OPLE so that seven OPLEs can be used with ten beam transfer tubes. The mirrors will be moved and adjusted by hand rather than remotely since the change of telescope positions will not occur frequently. Figure G.16 shows the layout for the beam director assembly. The primed telescope designation is the alternate position for that telescope, and the B positions of the directing mirrors are the ones for directing the beams from the alternate telescope positions into the OPLE.

FIGURE G.16. Layout of the beam director assembly.

Four $12'' \times 12''$ and three $24'' \times 24''$ optical table bread boards on concrete piers will support the mirrors with mirror mounts so that they can be reached for repositioning and adjustment.

G.4.8. Input–Output Mirror Assembly

The input and output mirrors for one OPLE are shown in Figure G.15. The set of mirrors, M_1 and M_2, direct the beam from the beam director assembly into the cat's eye and allow for a height adjustment between the two assemblies. Mirrors M_5 and M_6, take the return beam from M_3 that is in a horizontal plane and sends it back to M_3 so that it is returned in a vertical plane and is directed by mirrors, M_7 and M_8, to the next subsystem. Mirror M_1 is in a motorized mount for remote alignment. The supports for mirrors and mounts will be similar to those for the beam director. Figure G.17 shows the subassembly hardware trees for the beam director assembly and the input-output mirror assembly.

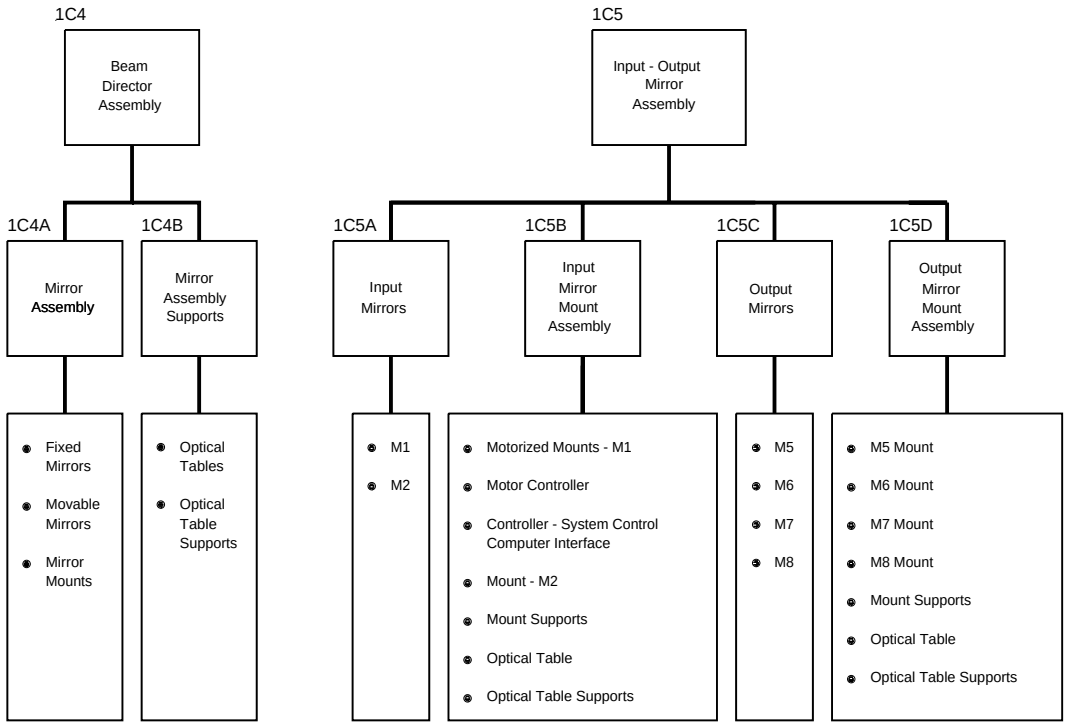

FIGURE G.17. OPLE beam director and input-output mirror subassemblies hardware trees.

G.4.9. Environmental Monitors

The environmental sensors will be placed in the OPLE room to measure temperature, pressure and relative humidity. The results of the measurements will be used to obtain an accurate and current value of the index of refraction of air using an expression determined by Jones that is given in the paper by Estler (1985). The correction will attempt to maintain the error of the LMA to the lower value given in the last column of Table G.1. These measurements will be sent to the subsystem computer at least every ten minutes to update a file that is used by the LMA to determine the positions and velocities of the OPLE mirror carts.

The temperature sensors will be bead thermistors that have been aged to reduce long-term drift. The thermistor will be read by a digital ohm meter which has a least count of ± 1 ohm. The digital ohm meter will also serve as the interface to the computer. If the thermistors are calibrated to an accuracy of 5 mK then it is expected that the temperature of the air can be measured to ± 0.01 K.

The atmospheric pressure will be measured with a flexible diaphragm capacitance-type transducer which produces a nearly linear 0-5 VDC over the range of 600-800 mm of Hg. A digital voltmeter with high resolution will read the voltage and serve as the interface to the monitoring computer. If the sensor is calibrated properly and the proper digital voltmeter is used, the pressure can be measured to ± 0.02 mm of Hg.

The relative humidity will be measured with a commercially available instrument that uses the principle of the chilled mirror dew-point hygrometer. The mirror is cooled below ambient temperature by a thermoelectric cooler, and the amount of condensation on the

surface is determined by measuring the surface reflectivity using a LED and photodiode detector. The condensation is kept constant by a feedback loop from the reflectivity sensor to the cooler current. The dew-point and ambient temperatures are measured by platinum resistance thermometers. The relative humidity is calculated from the relevant portion of the psychrometric chart that is contained in a PROM. The output of the instrument is a DC voltage and will be connected through a digital voltmeter or A/D converter board to the subsystem control computer. With the proper calibrations the relative humidity can be measured to $\pm 0.5\%$. Figure G.18 shows the environmental monitor subassemblies hardware tree.

G.4.10. Subsystem Controller

The computer controller assembly will supply the control and monitor functions for the OPLE subsystem. The general features of all the subsystem control computers are described in Appendix U of this report.

The main function of the control computer will be to manage the control of each of the OPLE cart positioning systems. The details of this system are not complete, but the general features can be given. As stated above, the OPLE cart position control has a stepper motor, a PZT driven flexure mirror support and a PZT that varies the position of the secondary mirror of the cat's eye with each of these transducers providing finer control and operating with a wider bandwidth control loop. However, each of the control loops will be cascaded so that stable control can be maintained. Although it might not be required, it may be operationally more robust to have each of the these systems work in multiples of a single clock. Since the LMA must be part of the overall control system, it should also operate on a multiple of the master clock. A possible scheme for this would be to have a master clock frequency of 104 Hz, the LMA and secondary at 103 Hz,, the flexure at 100 Hz and the stepper motor at 12.5 Hz. The control loop would be driven either by an astrometric model which is transferred from the system control computer or by corrections from the fringe tracker system which would use 100 Hz or less as an operational frequency.

The control computer will receive slewing commands from the system control computer and execute them via the cart control assembly. The subsystem control computer will record the environmental measurements, receive the metrology data from the LMA, and make the calculations that convert from air to vacuum wavelength. The subsystem control computer will send the environmental data as well as the OPLE position data to the system control computer for archival purposes. Finally, the subsystem control computer will move the mirror M_6, on commands from the system control computer so that a single operator at the system computer can manage alignment. Figure G.18 shows the controller computer subassemblies hardware tree.

G.5. REFERENCES

Davis, J., 1993, "The Sydney University Stellar Interferometer (SUSI) ", in *Proc: Iau Symp 158 on Very High Angular Resolution Astronomy,* Ed: W. J. Tango and G. Robertson, in press

Estler, W. T., 1985, "High-accuracy displacement interferometry in air", *Appl.Optics*, **24**, 808

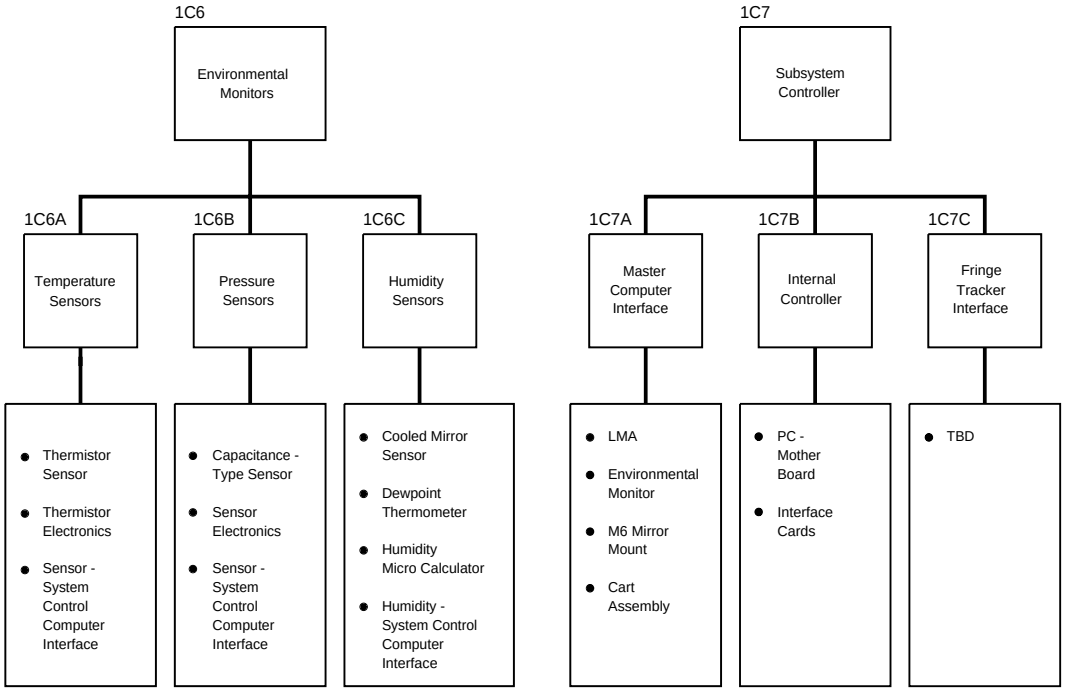

FIGURE G.18. OPLE environmental monitor and control computer subassemblies hardware trees.